New Primary Ice-Nucleation Parameterizations in an Explicit Cloud Model

MICHAEL P. MEYERS, PAUL J. DEMOTT, AND WILLIAM R. COTTON

Colorado State University, Department of Atmospheric Science, Fort Collins, Colorado

(Manuscript received 18 March 1991, in final form 25 November 1991)

ABSTRACT

Two new primary ice-nucleation parameterizations are examined in the Regional Atmospheric Modeling System (RAMS) cloud model via sensitivity tests on a wintertime precipitation event in the Sierra Nevada region. A model combining the effects of deposition and condensation-freezing nucleation is formulated based on data obtained from continuous-flow diffusion chambers. The data indicate an exponential variation of ice-nuclei concentrations with ice supersaturation reasonably independent of temperatures between $-7°$ and $-20°C$. Predicted ice concentrations from these measurements exceed values predicted by the widely used temperature-dependent Fletcher approximation by as much as one order of magnitude at temperatures warmer than $-20°C$. A contact-freezing nucleation model is also formulated based on laboratory data gathered by various authors using techniques that isolated this nucleation mode. Predicted contact nuclei concentrations based on the newer measurements are as much as three orders of magnitude less than values estimated by Young's model, which has been widely used for predicted schemes.

Simulations of the orographic precipitation event over the Sierra Nevada indicate that the pristine ice fields are very sensitive to the changes in the ice-nucleation formulation, with the pristine ice field resulting from the new formulation comparing much better to the observed magnitudes and structure from the case study. Deposition–condensation-freezing nucleation dominates contact-freezing nucleation in the new scheme, except in the downward branch of the mountain wave, where contact freezing dominates in the evaporating cloud. Secondary ice production is more dominant at warm temperatures in the new scheme, producing more pristine ice crystals over the barrier. The old contact-freezing nucleation scheme overpredicts pristine ice-crystal concentrations, which depletes cloud water available for secondary ice production. The effect of the new parameterizations on the precipitating hydrometeors is substantial with nearly a 10% increase in precipitation across the domain. Graupel precipitation increased dramatically due to more cloud water available with the new scheme.

1. Introduction

Meyers and Cotton (1992) applied the Regional Atmospheric Modeling System (RAMS) developed at Colorado State University (CSU) to simulate a wintertime orographic cloud system that occurred on 12 February 1986 over the Sierra Nevada (Fig. 1). The Sierra Cooperative Pilot Project (SCPP) (Reynolds and Dennis 1986) database documents the microphysical and precipitation evolution of this storm quite well. A detailed observational description of the case is given in Rauber (1992). The simulated results were compared to the observed kinematic structure, microphysical structure, and surface precipitation. The model predicted most of these parameters quite well, with the notable exception of pristine ice concentrations that were overpredicted by an order of magnitude in some regions. The microphysical model (Cotton et al. 1986) currently has three nucleation modes (or mechanisms)

to predict pristine ice concentrations: 1) a routine to estimate the combined contributions of deposition and condensation-freezing nucleation based on a modified Fletcher approximation, 2) contact freezing based on Young's (1974a) formulation, and 3) secondary ice production based on the Hallett–Mossop (Hallett and Mossop 1974) ice-multiplication process. This paper describes new parameterizations for the combined effects of deposition and condensation-freezing nucleation and for contact-freezing nucleation. Examination of the cloud model's response to the new predictive schemes is conducted and compared to the old schemes' results and to the observations. The 12 February 1986 case study is used to evaluate the sensitivity of the microphysical and precipitation structure to the choice of schemes.

2. Background

Regardless of the ultimate influence on predicted precipitation, it is at least aesthetically desirable to accurately predict initial ice concentrations when simulating clouds numerically. In some cases accurate initiation of primary and secondary ice processes are crit-

Corresponding author address: Michael P. Meyers, Colorado State University, Department of Atmospheric Science, Fort Collins, CO 80523.
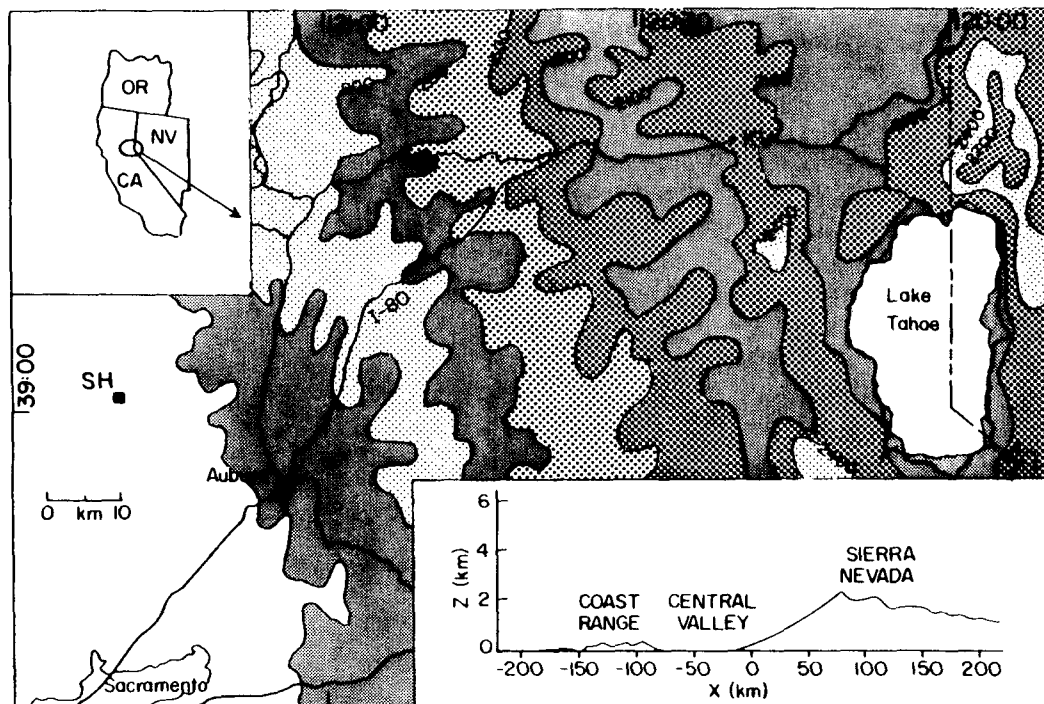
FIG. 1. Topographic map of the SCPP area (adapted from Rauber 1992), with a state map shown in the inset in the upper left, and a horizontal slice of topography used in simulation shown in the inset in the lower right.

ical to simulating precipitation and fields of water species (liquid water, graupel, aggregates), as well as the radiative properties of clouds. Knight (1990) describes a Lagrangian modeling simulation of an isolated cumulus first-echo case in which the specification of the ice-nucleus spectrum is one of the most critical elements. The prediction of primary ice-crystal concentrations in numerical cloud models is a difficult task since ice-nucleation activity in real clouds can be realized by way of various nucleation modes, which are still poorly understood. These modes are deposition nucleation, condensation freezing, contact freezing, and immersion freezing. The majority of measurements of ice-nucleus concentrations have been made with a variety of instruments for which the modes measured were not always well defined, and the temporal and spatial scatter of observed values is large. One approach when predicting ice-crystal concentrations has been to use a temperature-dependent function (i.e., Fletcher 1962) to predict concentrations based on the compilation of measured ice-nucleus concentrations (by all techniques). This method frequently underestimates potential ice-crystal concentrations compared to observations at warmer temperatures. Years of study of natural ice-crystal concentration measurements have been summarized by various authors (see, for example, Vali 1985a). Ice-concentration measurements in clouds where secondary ice-formation processes were believed to be unimportant exceed averages of various ice-nucleus measurements by as much as one order of magnitude or more at temperatures warmer than about $-20°C$ (Hobbs 1969; Koenig 1962; Mossop and Ono 1969; and Mossop et al. 1970, 1972). If the Fletcher formulation is extrapolated to temperatures below those for which it is valid (about $-25°C$), overprediction of ice-crystal concentration may occur. This makes the use of this formulation unsatisfactory for numerical cloud modeling. However, other data on ice-nucleation concentrations have become available that can be directly attributed to a single ice-nucleation mechanism, or a combination of these, and these newer data appear more consistent with ice-crystal concentrations attributable to primary ice-nucleation processes in many clouds.

This paper initiates an effort to systematically develop and implement new routines for ice-crystal formation by primary nucleation modes in the RAMS, based on what are subjectively deemed the most appropriate data available. This paper examines explicit nucleation by deposition and condensation freezing, a combined description of two mechanisms that are frequently grouped together due to their sensitivity to vapor concentration and contact-freezing nucleation.

a. Deposition and condensation-freezing nucleation

Deposition nucleation is defined as the "formation of ice in a (supersaturated) vapor environment" (Vali

1985b). This ice-formation process may hypothetically occur for any conditions exceeding ice saturation at freezing temperatures. Condensation-freezing nucleation is "the sequence of events whereby a CCN initiates freezing of the condensate" (Vali 1985b) by acting also as an ice nucleus. This suggests that condensation freezing requires conditions mostly exceeding water supersaturation at freezing temperatures. For these conditions, deposition nucleation may also occur. Without special experiments it is not possible in practice to distinguish the separate contributions of deposition and condensation freezing when a cloud parcel is supersaturated with respect to water. In this section we briefly review available measurements that have distinguished concentrations of natural deposition and condensation-freezing nuclei, and we propose the use of a single parameterization of ice formation to describe the combined contributions of these mechanisms in RAMS.

Various instruments that attempt to establish a known vapor concentration about particles either collected from air and supported on fiber filters or freely suspended in air have been used to estimate natural concentrations of deposition and condensation-freezing nuclei. In many filter processing devices (i.e., Gagin and Arroyo 1969) an ice surface over the filter provides a vapor source at a temperature warmer than the filter, and the saturation conditions at the filter surface can be calculated. The potential weaknesses and uncertainties of the filter method, primarily relating to rapid vapor depletion by collected cloud condensation nuclei (CCN) aerosols and growing ice crystals, are well documented (i.e., Huffman and Vali 1973; Zamurs et al. 1977). Ice-nuclei concentrations detected by the filter method are highly variable, and average values ($T > -20°C$) are much lower than ice-crystal concentrations attributable to primary ice nucleation in clouds. Measured values typically follow Fletcher's (1962) formula (see, e.g., Fig. 2) representing a composite of ice-nuclei measurements made with various devices that were nonspecific with regard to the ice-nucleation mechanism.

Several authors have improved the filter method by using a steady-state flow of air of controlled humidity above or directed at filters (e.g., Langer and Rodgers 1975; Saunders and Al-Juboory 1988), or by preventing aerosol exposure while steady-state supersaturation is established (Berezinskiy and Stepanov 1986). These improvements were meant to eliminate transient temperature and humidity-depletion effects. The improved filter methods have produced inconsistent results. Nevertheless, some of these measurements have indicated the existence of ice-nuclei concentrations an order of magnitude or more higher than the static method (i.e., approaching $10 \, l^{-1}$ at $-20°C$). Using such a device, Rosinski and Morgan (1988) also demonstrated that, although a slight water supersaturation causes the nucleation of higher concentrations of ice at any tem-

perature than one observes at water saturation or subsaturation, higher values of supersaturation do not appear to cause the nucleation of additional ice crystals. Their results were obtained for maritime aerosols.

Methods that provide for measurement of the sensitivity of ice nucleation from the vapor to ice or water supersaturation or both without the use of a supporting substrate should lead to the least ambiguous results. Schaller and Fukuta (1979) presented results from a wedge-shaped thermal-diffusion-chamber device, which allowed freely suspended aerosols to be exposed to a range of humidity conditions between ice saturation and water supersaturation at any chosen temperature. An important finding was the strong rise in nucleation activity with finite water supersaturations for known ice-nucleating substances, which they attributed to condensation-freezing nucleation. However, Schaller and Fukuta did not test natural aerosols.

Continuous-flow diffusion-chamber devices (Tomlinson and Fukuta 1985; Hussain and Saunders 1984; Rogers 1982, 1988) also measure ice nucleation without a supporting substrate. In these devices particles are forced to follow a flow channel between two temperature-controlled parallel or concentric cylindrical plates, so that they are exposed to the same humidity conditions (water subsaturated or water supersaturated) for a finite time. The flow design permits the processing of large sample volumes (implies higher sensitivity for measuring low ice-nuclei concentrations) and helps to ensure that ice-crystal and cloud-droplet growth do not deplete humidity significantly as measurements are made. Measurements of natural ice-nuclei concentrations with such devices are sparse. Nevertheless, a consistent feature of the measurements is that ice-nucleus concentrations are of a magnitude sufficient to explain ice-crystal concentrations in many types of atmospheric clouds, particularly at temperatures greater than $-20°C$. An example is given in Fig. 2. This figure compares the results from various mechanistic studies of ice-nuclei concentrations to the Fletcher curve and to measurements of ice in Elk Mountain (Wyoming) cap clouds in conditions for which primary nucleation was deemed the only potential source for ice crystals. Continuous-flow-device measurements of ice nuclei (R) appear to set an upper limit for the ice-crystal concentrations observed. The continuous-flow-device data of Rogers (1982) and Al-Naimi and Saunders (1985) are shown plotted as a function of ice supersaturation in Fig. 3. The data of Rogers show little temperature dependence to ice-nuclei concentration beyond that inherent with the range of ice supersaturations tested at any temperature. The data of Al-Naimi and Saunders show a direct relationship with absolute temperature for sub–water-saturated conditions. It is not clear if this is a characteristic of the air masses measured or an instrumental difference. On the whole, however, the strongest feature of the two datasets is the direct relationship between ice-nucleus
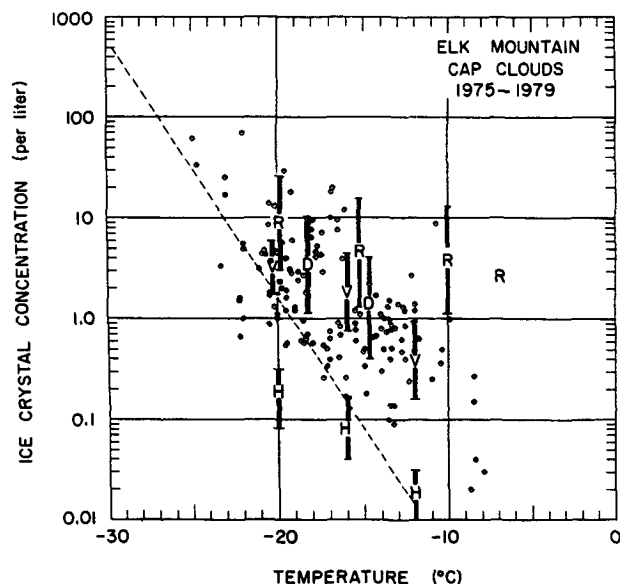
FIG. 2. Summary of ice-crystal concentration measurements in Elk Mountain cap clouds. Each aircraft data point (circle) represents a cloud penetration average (30 clouds on 26 days). Geometric means and standard deviations of ice-nucleus data are from (H) Huffman's (1973) membrane filter measurements, from (V) Vali's (1974 and 1976) and (D) Deshler's (1982) contact-freezing nucleus measurements, and from (R) Rogers (1982) continuous-flow diffusion chamber measurements. Fletcher's (1962) ice-nucleus curve is also shown for reference (– – –). The figure is adapted from Rogers (1982).

ice supersaturation, and $S_0 - 1$ is the fractional ice supersaturation at water saturation (at T_{sup}). Ice-crystal concentrations given by (2.3) at temperatures of $-10°$, $-15°$, and $-20°C$ and for a variety of ice supersaturations are shown in Fig. 3. The values predicted mostly represent the state of knowledge of natural ice-nuclei dependence on temperature and saturation ratio based on measurements other than continuous-flow-device measurements. Comparison to the continuous-flow measurements shows the potential inadequacy of such a treatment. For this study we choose to formulate a single expression for deposition and condensation-freezing nucleation using the results from the continuous-flow chamber studies. We do so because of the apparent advantages of the technique for accurately measuring concentrations of natural ice nuclei, and because the results representing the contributions of both mechanisms can be parameterized with little error as a simple function of ice supersaturation. Rogers (1982) noted this fact in his study. While Rogers demonstrated statistically that the ice-crystal concentrations nucleated at water subsaturations and those nucleated at water supersaturations were primarily from separate populations, a regression that treated the two populations together resulted in a correlation nearly as good as treating the populations separately. The potential weaknesses of this approach are that the number, tem-

concentration on ice supersaturation, independent of whether or not the air is subsaturated or supersaturated with respect to water. Another strong feature, which also supports the filter method results of Rosinski and Morgan (1988), is the lack of strong sensitivity of nucleation to the level of water supersaturation.

Concerned by the tendency of the Fletcher (1962) ice-nuclei formula to overpredict ice-crystal concentrations in very cold clouds, and with the lack of sensitivity of this formula to saturation conditions, Cotton et al. (1986) combined the Fletcher temperature-dependent formulation

$$N_{id} = N_0 \exp(aT_{sup}), \qquad (2.1)$$

with the Huffman (1973a,b) equation for the relative supersaturation dependence of ice nucleation (by the static filter method)

$$N_{id} = [(S_i - 1)(S_0 - 1)^{-1}]^b \qquad (2.2)$$

to obtain the hybrid equation

$$N_{id} = N_0[(S_i - 1)(S_0 - 1)^{-1}]^b \exp(aT_{sup}). \qquad (2.3)$$

In this equation, $a = 0.6°C^{-1}$, $b = 4.5$, $N_0 = 10^{-5} 1^{-1}$, T_{sup} is the degree of supercooling, $S_i - 1$ is the fractional
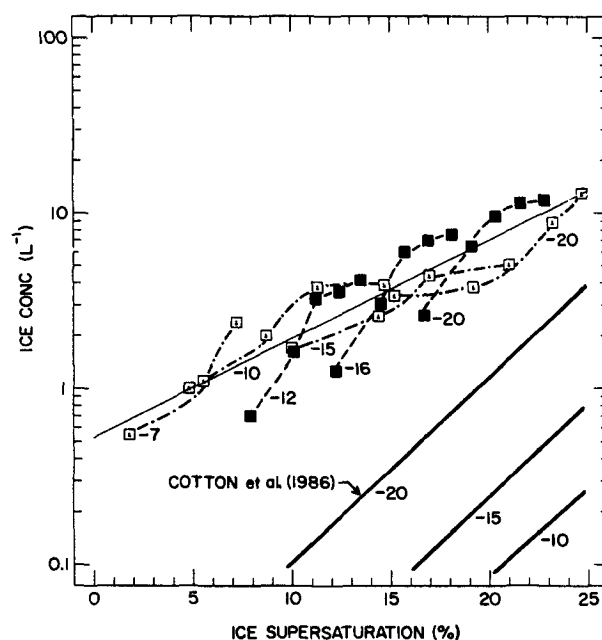

FIG. 3. Continuous-flow diffusion-chamber ice-nucleus concentration measurements versus ice supersaturation from (open square) Rogers (1982), and from (filled square) Al-Naimi and Saunders (1985). Constant-temperature measurement series are indicated and the regression given in (2.4) is shown. Also presented are constant temperature values predicted by the deposition–condensation-freezing nucleation model formulated by Cotton et al. (1986).

perature range, and locations (surface based only) of available measurements made with continuous-flow devices are limited and may not be wholly representative of the atmosphere. In fairness, however, no technique has yet provided a thorough mapping of accurate ice-nucleus concentrations spatially and temporally in the atmosphere. This stated, a parameterization of the measured ice-nucleus concentrations on ice supersaturation is given by

$$N_{id} = \exp\{a + b[100(S_i - 1)]\} \qquad (2.4)$$

where N_{id} (l^{-1}) is the number of pristine ice crystals predicted due to deposition–condensation freezing, $a = -0.639$, $b = 0.1296$. The square of the correlation coefficient for this fit is .82. The fit is shown by the solid line through the data in Fig. 3. The equation may be strictly applied over the temperature and supersaturation ranges of the data, which are from $-7°$ to $-20°C$, from 2% to 25% ice supersaturation, and from -5% to $+4.5\%$ water supersaturation. We use (2.4) in this study outside of these environmental ranges, but make note of the influence of this extrapolation in the results. Warm temperature nucleation is arbitrarily prevented at warmer than $-5°C$.

Recently, Hobbs and Rangno (1990) and Rangno and Hobbs (1991); (hereafter referred to as HR and RH, respectively) have hypothesized, based on measurements of ice-crystal concentration evolution made in a large number of maritime cumulus clouds, that conditions that produce higher than average conditions of water supersaturation in clouds lead to the spontaneous primary nucleation of ice crystals (on aerosol particles) in concentrations greater than 100 l^{-1} at cloud temperatures warmer than $-12°C$. The condition leading to water supersaturations of as much as 10%–15% is the onset of coalescence, as proposed and demonstrated numerically by Young (1974b). Using a one-dimensional microphysical model, Hall (1980) found similar results in a two-dimensional (2D) framework. The possibility of enhanced ice nucleation resulting from these transient high supersaturations by HR and RH has also been suggested by Cotton and Anthes (1989). This newer hypothesis replaces the suggestion by Hobbs and Rangno (1985) that thermophoretically enhanced contact-freezing nucleation in strong evaporation zones near cloud top might be the primary process responsible for the onset of rapid ice formation observed when substantial numbers of cloud droplets begin to exceed ~20 μm in diameter.

The data represented by (2.4) is relevant to the HR and RH hypothesis, so it is interesting to compare predicted values to their measurements. It is found that a water supersaturation of 27.5% is necessary to nucleate 100 l^{-1} ice crystals at $-10°C$. This value exceeds the estimates of transient water supersaturations that might occur during coalescence in supercooled clouds. How-

ever, measurements of spatial and temporal variations of ice-nuclei concentrations versus water supersaturation have not been made. Actual values may differ from and even exceed the few values measured at the surface using continuous-flow chambers. We must also note that, although (2.4) predicts higher ice-nuclei concentrations on extrapolation outside the measurement range for which it was derived (8 l^{-1} and 16 l^{-1} at 10% and 15% water supersaturation, respectively, at $-10°C$), the RAMS physics is not able to simulate the transient supersaturation effects proposed by HR and RH, since cloud-droplet concentration is not a predicted variable. This is a problem for future research.

b. Contact-freezing nucleation

There are not many measurements available that have attempted to specifically isolate contact-freezing nuclei concentrations. However, there are substantially more so than when Young (1974a) made his estimates of contact-freezing nuclei concentrations based on Blanchard's (1957) experiments. More recent relevant measurements are those of Vali (1974, 1976), Cooper (1980), and Deshler (1982).

Vali used an electrostatic precipitator to impact aerosols onto pure, supercooled water droplets. Since aerosol charging is strongly size dependent, Vali's instrument has good sampling efficiency for particles >0.1 μm, but not for particles <0.01 μm. His values given (V) in Fig. 2 and in Fig. 4 range from 0.4 to 3.2 l^{-1} at temperatures from $-12°$ to $-20°C$.

Deshler's technique relied on Brownian diffusion and phoretic forces to transport aerosols to the surface of pure supercooled water drops. The sampling rates of aerosols by this method are size dependent in the opposite sense to Vali's method, decreasing by a factor of 10 from 0.01 to 0.1 μm. Assuming diameters of 0.01, 0.05, and 0.1 μm, Deshler estimated concentrations in the range from 0.4 to 20 l^{-1} at $-15°$ and $-18°C$. These measurements (D) are shown in Fig. 2 (largest size is highest concentration). In Fig. 4 only the 0.1-μm concentrations values are shown. If the nuclei collected were larger, concentrations must have been higher.

Cooper collected particles onto membrane filters exposed to temperatures between $-10°$ and $-20°C$ and let supercooled droplets (~70 μm in diameter) fall on them. His method should be mostly independent of aerosol size. He reported concentrations between about 1 l^{-1} at $-10°C$ and 10 l^{-1} at $-20°C$. His results are given (C) in Fig. 4.

For comparison in Fig. 4, Young's (1974a) values, which were used previously in RAMS, are shown (Y). The experiments by Blanchard in which these values are based were performed in a wind tunnel. The measurements relied on the same physical processes as in Deshler's technique. These potential contact-freezing
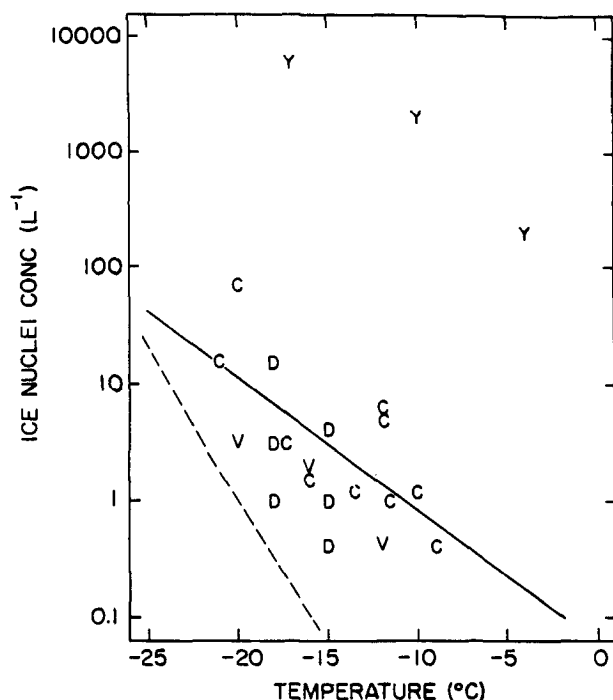
FIG. 4. Summary of measurements of contact-freezing ice-nuclei concentrations made by various authors (C, D, V) as discussed in text. For comparison, the estimates of Young (1974a) (Y) are shown. The regression line is an exponential fit to measurements. Fletcher's (1962) ice-nucleus curve is also shown for reference (– – –).

nuclei concentrations were parameterized by Young (1974b) in the form

$$N_{ic} = N_{a0}(270.16 - T_c)^{1.3} \qquad (2.5)$$

where T_c is the cloud-droplet temperature and N_{a0} = 2.0×10^2 l^{-1} at sea level. Young assumed N_{a0} decreased linearly with height to 10 l^{-1} at 5000 m MSL in numerical simulations of wintertime orographic clouds. Cotton et al. (1986) assumed $N_{a0} = 2.0 \times 10^2$ l^{-1} at all levels. In making his estimates Young presumed that the nuclei must be large (~ 1 μm in diameter). Collection rates were thus very small and concentrations had to be very high. The results obtained by Vali and Cooper appear to invalidate Young's assumption. High concentrations of large contact-freezing nuclei do not appear to exist in their data.

We therefore choose to quantify contact-freezing nuclei concentrations by fitting a function to the measurements of Vali (1974, 1976), Cooper (1980), and the values given by Deshler (1982), assuming aerosols are 0.1 μm in diameter. The choice of the functional fit to these data is probably not critical due to the spread in the data and the probable natural temporal and spatial variability in the concentrations. Therefore, an exponential of the form

$$N_{ic} = \exp[a + b(273.15 - T_c)], \qquad (2.6)$$

where $a = -2.80$ and $b = 0.262$, is used [units of N_{ic} are inverse liters (l^{-1})]. The square of the correlation coefficient is .52 for the fit of a and b, as presented in Fig. 4. Ice is not permitted to form by this mode of nucleation at temperatures warmer than $-2°$C. This function sets the upper limit to the potential ice-crystal concentration, which can be realized at any temperature by contact freezing. Collection rates determine the actual numbers nucleated. Collection occurs by Brownian, thermophoretic, and diffusiophoretic forcing following Young (1974a,b) with simplifications described in Cotton et al. (1986). A contact-freezing nuclei size of 0.1-μm radius is assumed.

3. Case study

The microphysical and kinematic structures of this case study are described in detail by Rauber (1992). The cloud system that affected central California on 12 February 1986 originated over the south-central Pacific and was characterized by warmer than normal temperatures ($T_{500 mb} = -16°$C). The flow was predominantly southwesterly, with 500-mb winds from 250° at 25 m s^{-1}, and 700-mb winds slightly backing to 225° at 20 m s^{-1}. A 25 m s^{-1} barrier jet (Parish 1982) was observed in the lowest kilometer. A series of short waves were embedded in the southwesterly flow, with the focus of the numerical experiment being initiated after the passage of a weak trough at 1500 UTC. Precipitation was observed over the length of the Sierra barrier and extended westward to the coast. Maximum precipitation amounts were observed 40 km upwind of the Sierra Nevada crest. A conceptual model of the precipitation processes observed in this case study is shown in Fig. 5. The schematic shows a moist fetch of cloud water being advected up the barrier in the lowest 2 km. Pristine ice crystals that are nucleated at colder temperatures advect downstream toward the barrier. The pristine ice crystals intersect a region of supercooled liquid water halfway up the barrier where rimed particles were observed. It is inferred from observations that secondary ice production due to rime splintering may have occurred in this region. Dendritic aggregates and dendritic–needle aggregates were observed near the top of the barrier up to an altitude of 4 km MSL and extended upstream toward the Central Valley. The top of the orographic cloud was observed at 5.5 km MSL, but an upper cloud deck was present at a higher altitude (estimated at 8 km MSL) based on rawinsonde and satellite data.

4. Experimental design

a. RAMS features used

The numerical model used in this study is a version of the RAMS cloud model developed at CSU (Tripoli
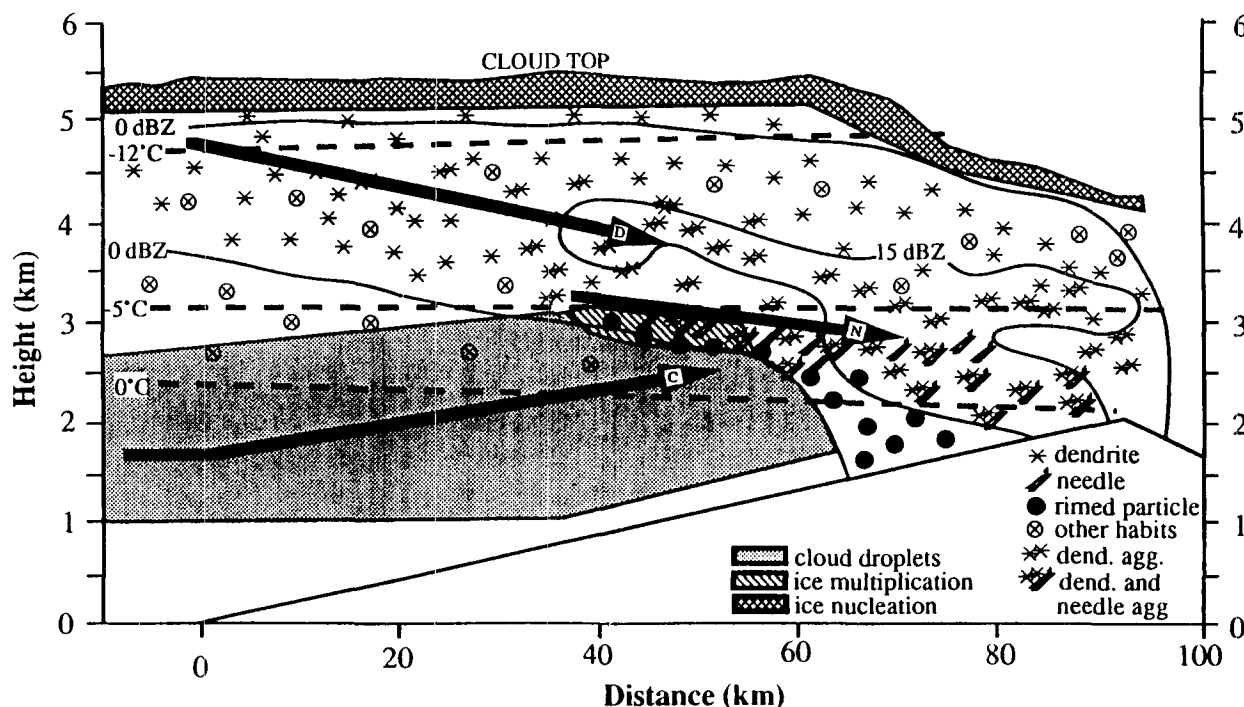
FIG. 5. Conceptual model of the microphysical processes occurring in the orographic cloud system. Arrows indicate cloud-droplet (C), needle (N), and dendritic-particle (D) trajectories in the plane of the cross section. Key isotherms (dashed) are also shown (from Rauber 1992).

and Cotton 1982; Cotton et al. 1982, 1986). RAMS is configured similar to Meyers and Cotton (1992) using the nonhydrostatic, fully compressible momentum equations, a thermodynamic energy equation, and equations for liquid- and ice-phase precipitation processes. The predicted variables include the three velocity components, the Exner function π, the ice–liquid water potential temperature θ_{il} (Tripoli and Cotton 1981), pristine ice-crystal concentrations, and mixing ratio of total water, rainwater, pristine ice crystals, graupel particles, and aggregates (Cotton et al. 1986). Potential temperature, temperature, cloud-droplet mixing ratio, water vapor mixing ratio, and pressure are calculated diagnostically (Tripoli and Cotton 1982). A flow diagram of the microphysical processes used in the model is given in Fig. 6. A comprehensive overview of the microphysics model is given in Flatau et al. (1989). Horizontal and vertical turbulence are parameterized using an eddy-viscosity closure scheme, as described by Tripoli and Cotton (1982). The equations are integrated numerically by a time-splitting procedure for a nonhydrostatic, compressible system (Tripoli and Cotton 1982) with a large time step of 5 s and a small time step of 2.5 s. Since mountain waves play an important role in determining the flow fields in orographic clouds, the Klemp and Durran (1983) radiative-type top boundary condition was used. The lateral boundary conditions employed were the Klemp

and Wilhelmson (1978) radiative type, together with a mesoscale compensation region outside the simulation domain (Tripoli and Cotton 1982). A terrain-following sigma-z vertical coordinate system is used following Gal-Chen and Somerville (1975a,b).

The model domain is 450 km long and 14.5 km in the vertical (Fig. 1). The horizontal grid resolution is 1.5 km and the vertical grid resolution is 0.25 km in the lowest levels up to the barrier crest and stretched to a constant vertical resolution of 0.5 km above 10 km. In order to adjust the flow over the mountain barrier, the model is dynamically initialized by adding the winds incrementally during the first 30 min as described by Tripoli and Cotton (1989). The model is then allowed to adjust to these winds for a 2.5-h period during which time all microphysical tendencies are deactivated. Cloud water, however, is allowed to form when saturation occurs. At 3.0 h the full microphysics module is activated.

b. Numerical experiments

To isolate the sensitivity of the model to the specific modes of primary nucleation, individual tests are run to 4 h. The simulations, as described briefly in Table 1, are run with one mode of primary ice nucleation activated (deposition–condensation freezing or contact-freezing nucleation) and allow comparisons be-
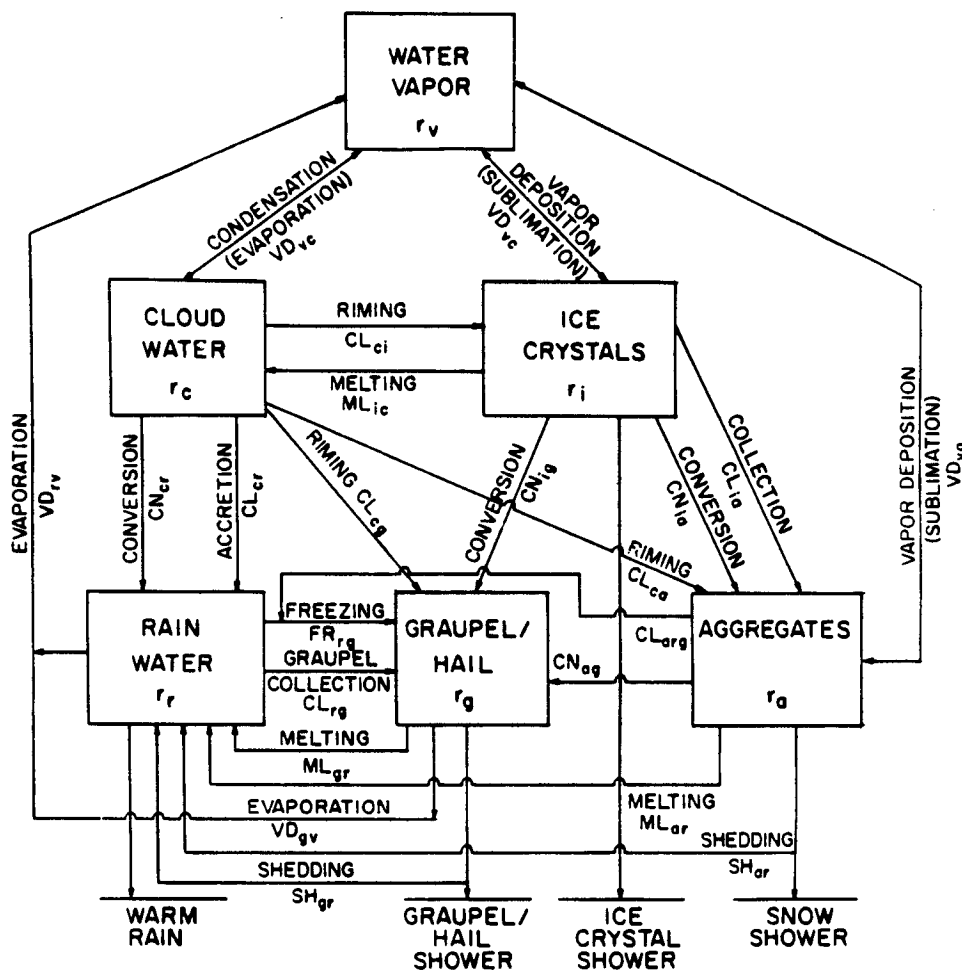
FIG. 6. Flow diagram describing microphysical processes considered in the model. The source and sink terms are defined as CN for conversion, ML for melting, FR for freezing, CL for collection, VD for vapor deposition or evaporation, SH for liquid water shedding. Each term includes a double subscript, where the first subscript is the water phase being depleted and the second subscript is the water phase which is growing. The subscripts v, c, r, i, g, and a refer to vapor, cloud, rain, pristine ice crystal, graupel, and aggregate water species, respectively.

tween the old and new parameterizations based on (2.3)–(2.6). Following the preliminary simulations are two production experiments run to 6 h comparing the old to the new physics. These production simulations include activation of the three modes of ice nucleation in RAMS: 1) deposition–condensation freezing, 2) contact freezing, and 3) secondary ice production. Examination of other microphysical fields and precipitation distributions are conducted in these production runs.

5. Results

a. Individual tests

In the following numerical experiments only one mode of ice nucleation is activated to examine the sen-

sitivity of the model to each specific mode of nucleation. Comparisons of both deposition–condensation freezing and contact-freezing nucleation modes are

TABLE 1. Short description of experiments.

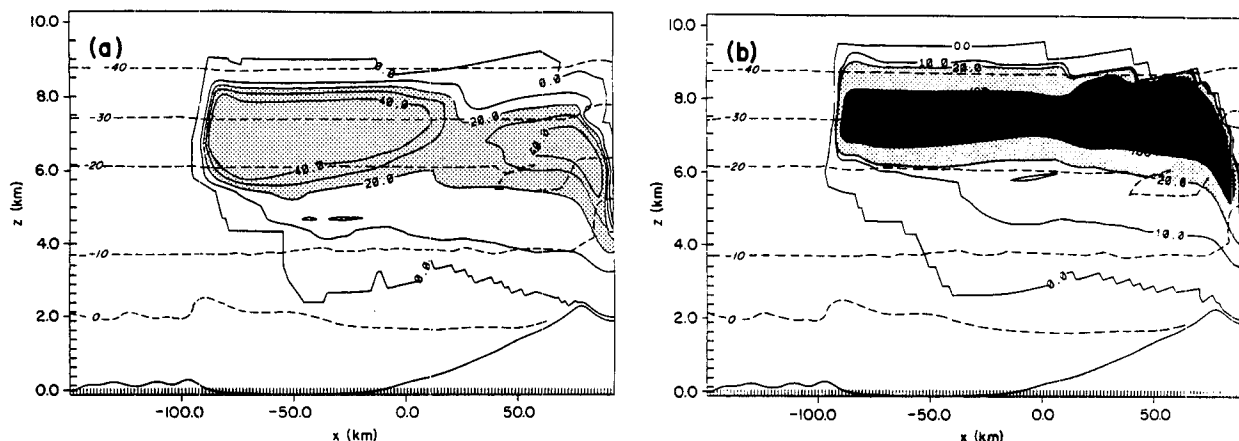|	Deposition–condensation–freezing scheme based on (2.3)	Deposition–condensation–freezing scheme based on (2.4)	Contact-freezing scheme based on (2.5)	Contact-freezing scheme based on (2.6)
EXP1			●	
EXP2	●			
EXP3				●
EXP4			●	
EXP5		●		●
EXP6	●		●	

FIG. 7. Predicted pristine ice concentration at 4 h for preliminary tests including deposition–condensation freezing with (a) new scheme, maximum value is 76 l^{-1}; (b) old scheme, maximum value is 900 l^{-1}. Contour interval is 10.0 l^{-1}. Values greater than 20 l^{-1} are light shaded and values greater than 100 l^{-1} are dark shaded. Isotherms at 10°C are also shown (- - -). The abscissa and ordinate are in kilometers.

discussed with emphasis on the impact on the pristine ice concentration and structure.

1) COMPARISON OF DEPOSITION-CONDENSATION-FREEZING SCHEMES

The pristine ice concentrations from the individual tests at 4 h with deposition–condensation freezing as the only nucleation process activated are shown in Fig. 7. The most dramatic difference is that pristine ice concentration values near 8 km MSL are predicted as high as 900 l^{-1} with EXP2 (old physics), while predicted pristine ice concentrations with EXP1 (new physics) are less than 100 l^{-1} (peak values 74 l^{-1}). The high values predicted in EXP2, located near the −35°C isotherm, are due to the strong dependence on supercooling of the modified Fletcher equation, shown in (2.3). It is worth restating that the modified Fletcher formulation is based on measurements that are not mode specific, but represents a questionable extrapolation of data for temperatures below −25°C, so it probably overpredicts deposition–condensation freezing at colder temperatures. Another region of interest that is more important for precipitation processes is in lower altitudes where higher quantities are predicted with the new scheme. In EXP1 concentrations of 2–10 l^{-1} are evident between 3 and 5 km MSL, which is well correlated to the values predicted by the data in Fig. 3 for temperatures between −5° and −20°C. Pristine ice concentrations predicted with the old scheme are much less at these warmer temperatures with values less than 2 l^{-1} at 4 km MSL. Another contrasting region between the two schemes is over the Coast Range where pristine ice concentrations up to 6 l^{-1} are predicted by the new scheme with none predicted by the old scheme. The effects of the dry midtroposphere between 5 and 6 km MSL are predicted more realistically with the new scheme. Concentrations with the old scheme at 5.5 km MSL are nearly twice those predicted in EXP1, consistent with a more pronounced sensitivity to ice supersaturation with the new scheme.

2) COMPARISON OF CONTACT-FREEZING SCHEMES

These simulations are run with contact-freezing nucleation as the only mode of ice nucleation activated. Pristine ice concentrations are shown in Fig. 8. Pristine ice crystals produced by contact-freezing nucleation are not as numerous as those predicted by deposition–condensation freezing (Fig. 7). In EXP3 (new physics) concentrations greater than 1 l^{-1} are confined between 4 and 8 km MSL over the extent of the barrier with peak values of 7 l^{-1} near the −20°C isotherm. This location is near the downward branch of the mountain wave where evaporation is prevalent. EXP4 (old physics) exhibits dramatic differences from EXP3 with pristine ice concentrations greater than 1 l^{-1} occurring over a much broader area. The pristine ice-crystal field is confined between 3 and 8 km MSL extending from the Coast Range to the Sierra crest, with peak values of 16 l^{-1} found between the −10° and −15°C isotherms. Note the location of the 10 l^{-1} contour from EXP4 is displaced upstream from the 1 l^{-1} contour in EXP3.

b. Comparison of production runs

In the individual tests the predicted pristine ice-crystal concentrations were quite sensitive to the changes in both the deposition–condensation-freezing and contact-freezing modes of nucleation. The deposition–condensation-freezing nucleation schemes dominated pristine ice nucleation especially at the higher levels (Fig. 7). At the middle and lower levels the deposition–
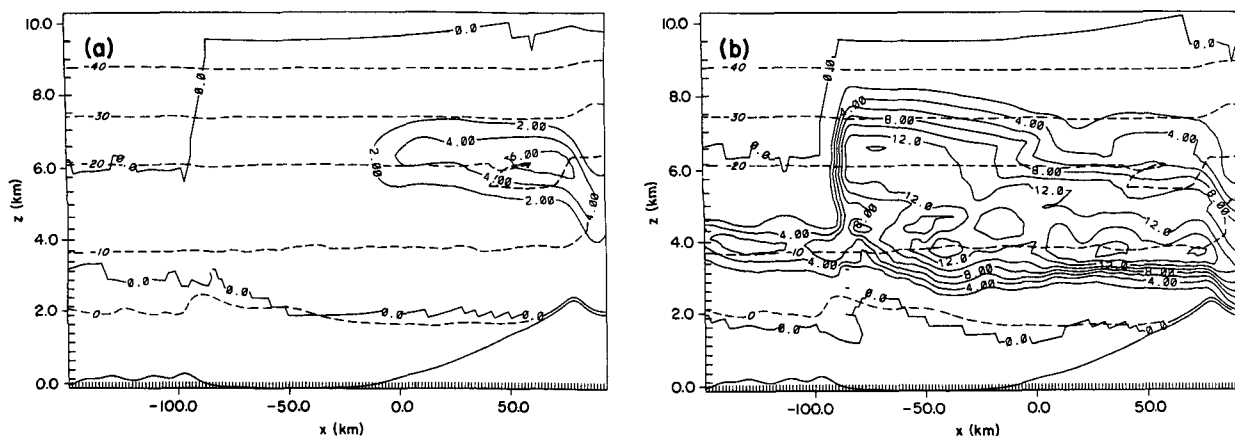
FIG. 8. Predicted pristine ice concentration at 4 h for preliminary tests for contact-freezing nucleation with (a) new scheme, maximum value is 6 l^{-1}; (b) old scheme, maximum value is 16 l^{-1}. Contour interval is 2.0 l^{-1}. The abscissa and ordinate are in kilometers. Isotherms at 10°C are also shown (– – –). The abscissa and ordinate are in kilometers.

condensation-freezing scheme dominated nucleation in the new scheme (Fig. 7a), while contact-freezing nucleation was dominant in the old scheme (Fig. 8b). In the following experiments deposition–condensation-freezing nucleation, contact-freezing nucleation, and secondary ice production are included, with the simulations run to 6 h. Predicted pristine ice concentrations for both experiments are shown in Fig. 9. Above 6 km MSL the structure of the two runs is similar, but EXP6 predicts three times as many ice crystals as EXP5. Peak values of 150 l^{-1} (Fig. 9b) are found near 7 km MSL over the barrier crest. Pristine ice concentrations of 50 l^{-1} are found in the same region from EXP5 (Fig. 9a). The drastic reduction of the 8-km MSL pristine ice maximum seen in EXP2 (peak value of 900 l^{-1}) as compared to EXP6 (peak value of 150 l^{-1}) is due to the increased competition for vapor when

all three nucleation modes are activated in EXP6. Below 5 km MSL (Fig. 9b) EXP6 exhibits higher values of pristine ice concentrations, which extend farther upstream over the Coast Range than predicted in EXP5. These higher values in EXP6 are due to the influence of the old, and we believe erroneous, contact-freezing nucleation scheme. Isolated peaks of pristine ice-crystal concentrations (50 l^{-1}) are evident near the −5°C isotherm above the barrier in EXP5, which are produced by secondary ice production. This feature is not as evident in EXP6 (Fig. 9b) because the old contact-freezing nucleation scheme tends to overnucleate at these temperatures, removing the cloud water needed for secondary ice production to occur. Measured pristine ice concentrations from this case study (Rauber 1992) range from 10 to 50 l^{-1}, which are predicted quite well by EXP5. These higher observed values are located
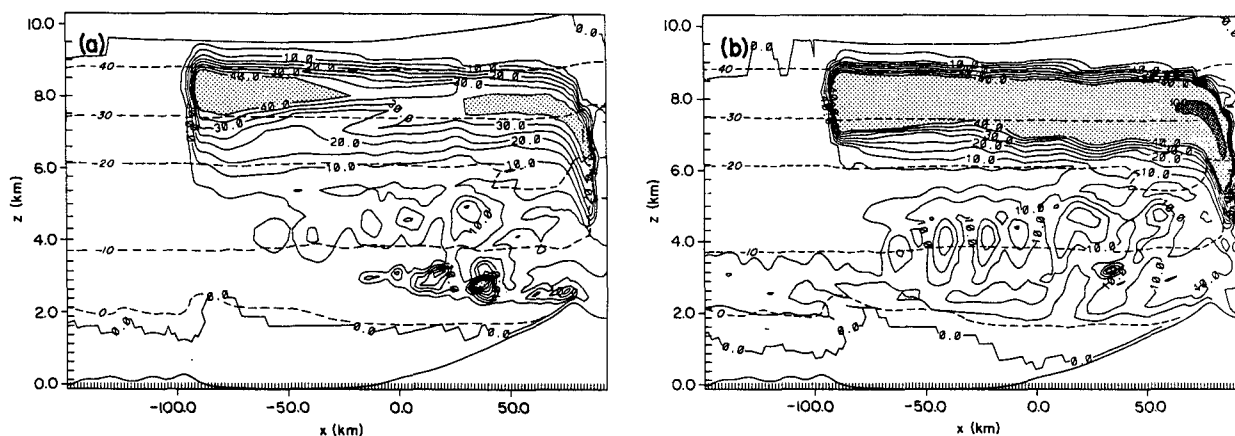

FIG. 9. Predicted pristine ice concentration at 6 h for production runs with (a) new scheme, maximum value is 50 l^{-1}; (b) old scheme, maximum value is 150 l^{-1}. Contour interval is 5.0 l^{-1}. Values greater than 40 l^{-1} are light shaded and values greater than 100 l^{-1} are dark shaded. The abscissa and ordinate are in kilometers. Isotherms at 10°C are also shown (– – –). The abscissa and ordinate are in kilometers.
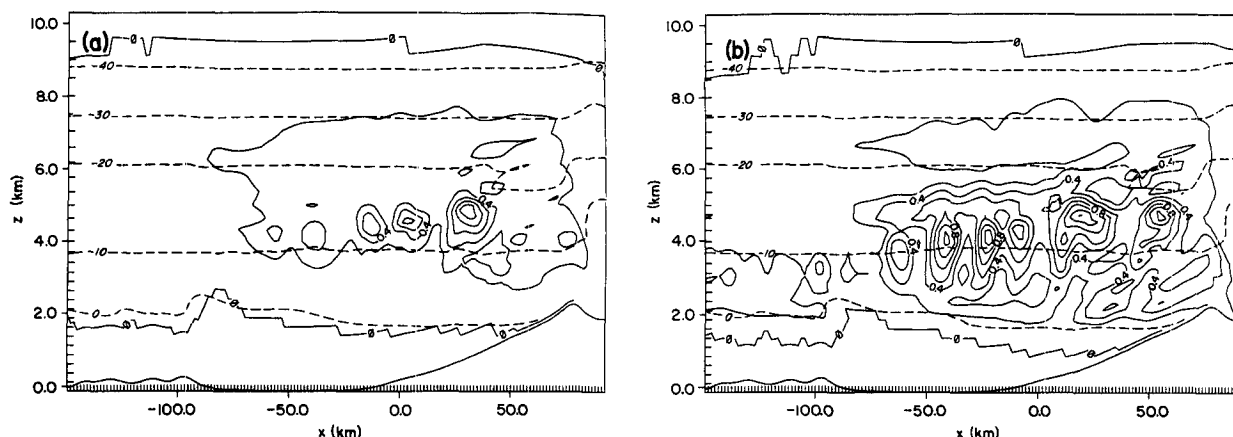
FIG. 10. Simulated pristine ice-crystal mixing-ratio fields at 6 h for (a) new scheme, maximum value is 1.0 g kg^{-1}; (b) old scheme, maximum value is 1.4 g kg^{-1}. Contour interval is 0.2 g kg^{-1}. The abscissa and ordinate are in kilometers. Isotherms at 10°C are also shown (– – –). The abscissa and ordinate are in kilometers.

where secondary ice production was inferred and predicted to occur.

The effects of the different schemes on the pristine ice mixing-ratio field are shown in Fig. 10. With the new deposition–condensation-freezing parameterization in EXP5, fewer pristine ice crystals are predicted (Fig. 9). The pristine ice mixing-ratio fields exhibit a similar signature with much less pristine mass being predicted in EXP5 (Fig. 10a). The old scheme predicts higher amounts over a deeper layer and farther upstream than was observed. The observed structure (Fig. 5) shows pristine mass to concentrate in the region just below the observed liquid cloud top, which is located near the 3 km MSL level. This feature is predicted quite well by EXP5; however, EXP6 predicts significant pristine ice-crystal mass (0.4 g kg^{-1}) near 2 km MSL, nearly 1.0 km lower than the observed location. The pristine ice-mass coverage is much more extensive in EXP6, due mostly to the old contact-nucleation scheme that predicted anomalously high amounts of pristine ice crystals in this region. The midtropospheric structure of both EXP5 and EXP6 are very similar to the observed structure (Fig. 5), which shows pristine ice crystals extending to top of the orographic cloud near 5.5 km MSL. An upper cloud deck is observed above this lower cloud existing up to 8 km MSL. EXP6 (Fig. 10b) shows more pristine ice mass being advected into the downward branch of the mountain wave, in a trajectory that avoids precipitation processes lower in the cloud. This characteristic of the pristine ice field may be a result of the assumed monodispersed size spectrum for pristine ice crystals (with respect to diameter) in the model. For a given mass, if more pristine ice crystals are predicted, the diagnosed mean diameter would be drastically smaller. With small terminal velocities, horizontal advection of pristine ice crystals is exaggerated, which allows advection of the ice crystals into

the downward branch of the mountain wave before influencing precipitation processes on the windward slope.

The structure of the simulated precipitation distributions comparing the two experiments is shown in Fig. 11. The total precipitation distributions (Fig. 11a) appear to be quite similar, with the heaviest amounts over the Sierra barrier decreasing to the lee of the barrier. Maximum precipitation amounts from the simulations are located halfway up the barrier, which is very similar to the observed distribution. EXP5, however, predicts 7% more precipitation on the windward side of the Sierra barrier than EXP6. These differences are significant considering that the previous study by Meyers and Cotton (1991) showed that the precipitation distribution was only slightly sensitive to modification of other microphysical parameters. Due to its long, gradual windward slope, the Sierra barrier is so efficient for precipitation processes that it is relatively insensitive to changes in the microphysics. The percentage of frozen precipitation is 36% in the new scheme, 6% greater than predicted in EXP6. Farther upstream from the barrier, 17% more precipitation fell in EXP5 than in EXP6. This difference can be attributed to the higher pristine ice mass produced by the old scheme in EXP6 upstream of the barrier, which depleted available cloud water from the precipitating hydrometeors. The precipitation distributions for rain, aggregates, and graupel are shown in Figs. 11b–d. The rain precipitation distribution (Fig. 11b) shows 15% more rain falling upstream of the Sierra barrier in EXP5 than in EXP6, with nearly equal amounts falling over the barrier. The peak amounts for EXP6 are slightly higher up the barrier than in EXP5. The aggregate precipitation distribution (Fig. 11c) is very similar between the two simulations with slightly more aggregate precipitation predicted in EXP5 over the Sierra crest. The
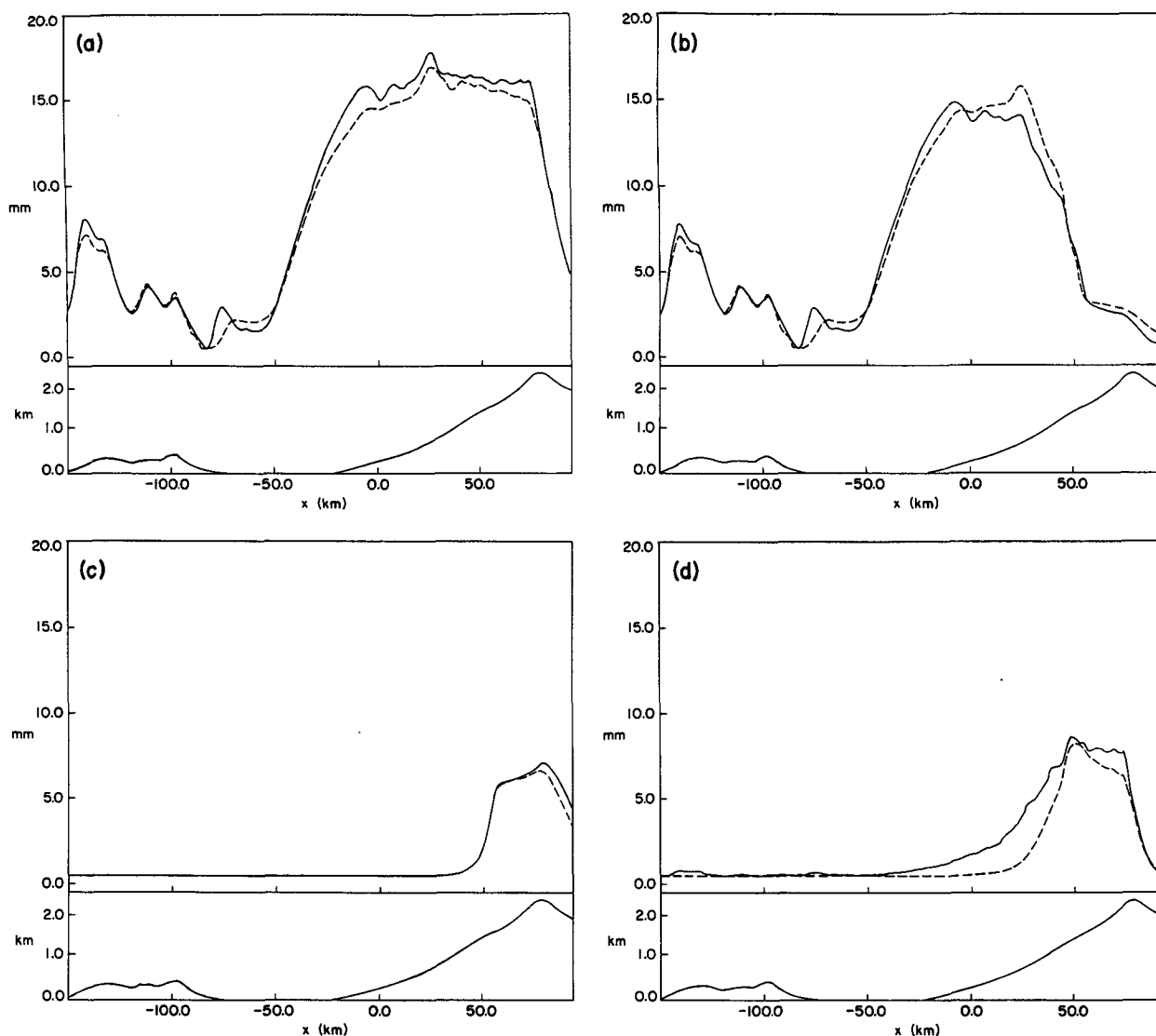
FIG. 11. Precipitation distribution for 3-h period of new scheme (solid lines) and old scheme (dashed lines) for (a) total precipitation, (b) rain precipitation, (c) aggregate precipitation, (d) graupel precipitation, with topography distribution centered below. Ordinate is precipitation amount in millimeters.

graupel precipitation distribution (Fig. 11d) shows the greatest differences between the two simulations with 30% more graupel precipitation falling over the barrier, using the new nucleation scheme. In both EXP5 and EXP6, the peak graupel precipitation occurs lower on the barrier than the aggregate precipitation, as also observed (see Fig. 5).

6. Conclusions

This study has described the impact of new deposition–condensation-freezing and contact-freezing models of ice nucleation on a numerical simulation of an orographic precipitation event. The new model of deposition–condensation-freezing nucleation is based on data obtained in continuous-flow diffusion-chamber studies, where the combined contributions of deposition and condensation-freezing nucleation are considered. These studies have measured potential deposition and condensation-freezing ice-nuclei (IN) concentrations an order of magnitude or greater than those measured by previous methods at temperatures warmer than −20°C. The new parameterization is compared here with a modified Fletcher formulation, the basis for the old deposition–condensation-freezing scheme in RAMS. The new model for contact-freezing nucleation is based on recent direct measurements of natural contact-freezing nuclei concentrations. These measured

concentrations were unavailable to Young (1974a) and are as much as several orders of magnitude less than his estimates, which were the basis for the old contact-freezing parameterization in RAMS.

Comparison of new and old nucleation schemes was made in simulations with RAMS of the 12 February 1986 wintertime orographic precipitation event over the Sierras. The predicted microphysical fields were very sensitive to modifications of the two modes of primary nucleation. The impact of changing from a modified Fletcher approximation to the new deposition–condensation-freezing model of nucleation produced higher concentrations and more mass of pristine ice at temperatures warmer than $-20°C$, this substantially altered the ice–water budget of the precipitating cloud. Predicted pristine ice concentrations at colder temperatures ($-35°C$) were significantly reduced with the new scheme. The new contact-freezing nucleation model removed the anomalous widespread prediction of pristine ice crystals produced by the old scheme at warmer temperatures ($-20°C$). Contact-freezing nucleation is now relegated to secondary importance. The overall structure and magnitude of the pristine ice-crystal field predicted by the new scheme compared more favorably with the observations. With fewer pristine ice crystals predicted at warmer temperatures with the new contact-freezing nucleation scheme, more cloud water was available enabling secondary ice multiplication to be an important mechanism near the barrier as observed. Pristine ice concentrations up to $50 \ l^{-1}$ were predicted above the barrier similar to the observed measurements. These changes in the pristine ice structure significantly altered the precipitating hydrometeors resulting in nearly a 10% increase in total precipitation across the domain. Graupel precipitation showed the greatest sensitivity to the new scheme, increasing by 30% over the barrier.

Future studies will examine the sensitivity of the new schemes on a sharper, less efficient barrier, such as the Colorado Rockies. Application to convective clouds will also be studied. Other research will address sensitivity to mechanisms, which may be particularly important in colder clouds such as cirrus. In particular, a model for homogeneous freezing of cloud water is being implemented. Because the results of this study exhibit a strong sensitivity to ice-nuclei estimates at supersaturations beyond the range of validity of the measurements, we urge that measurements of IN with new devices be obtained over a broader parameter space than has been done thus far.

REFERENCES

Al-Naimi, R., and C. P. R. Saunders, 1985: Measurements of natural deposition and condensation-freezing ice nuclei with a continuous flow chamber. *Atmos. Environ.,* **19,** 1871–1882.

Berezinskiy, N. A., and G. V. Stepanov, 1986: Dependence of the concentration of natural ice-forming nuclei of different size on the temperature and supersaturation. *Isvestiya, Atmos. and Oceanic Phys.,* **22,** 722–727.

Blanchard, D. C., 1957: The supercooling freezing and melting of giant water drops at terminal velocity in air. *Artificial Simulation of Rain,* Pergamon Press, 233–249.

Cooper, W. A., 1980: A method of detecting contact ice nuclei using filter samples. Preprints, *Eighth International Conf. on Cloud Physics,* Clermont-Ferrand, France, 665–668.

Cotton, W. R., and R. A. Anthes, 1989: *Storm and Cloud Dynamics.* Academic Press, 883 pp.

——, M. A. Stephens, T. Nehrkorn, and G. J. Tripoli, 1982: The Colorado State University three-dimensional cloud/mesoscale model—1982. Part II: An ice phase parameterization. *J. Rech. Atmos.,* **16,** 295–320.

——, G. J. Tripoli, R. M. Rauber, and E. A. Mulvihill, 1986: Numerical simulation of the effects of varying ice crystal nucleation rates and aggregation processes on orographic snowfall. *J. Climate Appl. Meteor.,* **25,** 1658–1680.

Deshler, T., 1982: Contact ice nucleation by submicron atmospheric aerosols. Ph.D. dissertation, Dept. of Physics and Astronomy, University of Wyoming, 107 pp.

Flatau, P. J., G. J. Tripoli, J. Verlinde, and W. R. Cotton, 1989: The CSU–RAMS cloud microphysical module: General theory and code documentation. Atmospheric Science Paper No. 451, 88 pp. [Available from Colorado State University, Dept. of Atmospheric Science, Fort Collins, Colorado 80523.]

Fletcher, N. H., 1962: *Physics of Rain Clouds.* Cambridge University Press, 386 pp.

Gal-Chen, T., and R. C. J. Somerville, 1975a: On the use of a coordinate transformation for the solution of the Navier–Stokes equations. *J. Comp. Physics,* **17,** 209–228.

——, and ——, 1975b: Numerical solution of the Navier–Stokes equations with topography. *J. Comp. Physics,* **17,** 276–310.

Gagin, A., and M. Arroyo, 1969: A thermal diffusion chamber for the measurement of ice nuclei concentrations. *J. Rech. Atmos.,* **4,** 115–122.

Hall, W. D., 1980: A detailed microphysical model within a two-dimensional dynamic framework: Model description and preliminary results. *J. Atmos. Sci.,* **37,** 2486–2507.

Hallett, J., and S. C. Mossop, 1974: Production of secondary ice particles during the riming process. *Nature,* **249,** 26–28.

Hobbs, P. V., 1969: Ice multiplication in clouds. *J. Atmos. Sci.,* **26,** 315–318.

——, and A. L. Rangno, 1985: Ice particle concentrations in clouds. *J. Atmos. Sci.,* **42,** 2523–2549.

——, and ——, 1990: Rapid development of high ice particle concentrations in small polar maritime cumuliform clouds. *J. Atmos. Sci.,* **47,** 2710–2722.

Huffman, P. J., 1973a: Supersaturation dependence of ice nucleation by deposition for silver iodide and natural aerosols. Report No. AR 108, 29 pp. [Available from University of Wyoming, Department of Atmospheric Resources, Laramie, Wyoming.]

——, 1973b: Supersaturation spectra of AgI and natural ice nuclei. *J. Appl. Meteor.,* **12,** 1080–1087.

——, and G. Vali, 1973: The effect of vapor depletion on ice nucleus measurements with membrane filters. *J. Appl. Meteor.,* **12,** 1018–1024.

Hussain, K., and C. P. R. Saunders, 1984: Ice nucleus measurement with a continuous flow chamber. *Quart. J. Roy. Meteor. Soc.,* **110,** 75–84.

Klemp, J. B., and J. Wilhelmson, 1978: The simulation of three-dimensional convective storm dynamics. *J. Atmos. Sci.,* **35,** 1070–1096.

——, and D. R. Durran, 1983: An upper boundary condition permitting internal gravity wave radiation in numerical mesoscale models. *Mon. Wea. Rev.,* **111,** 430–444.

Knight, C. A., 1990: Lagrangian modeling of the ice process: A first-echo case. *J. Appl. Meteor.,* **29,** 418–428.

Koenig, L. R., 1962: Ice in the summer atmosphere. Ph.D. thesis, Univ. of Chicago.

Langer, G., and J. Rodgers, 1975: An experimental study of the detection of ice nuclei on membrane filters and other substrata. *J. Appl. Meteor.,* **14,** 560–570.

Meyers, M. P., and W. R. Cotton, 1992: Evaluation of the potential for wintertime quantitative precipitation forecasting over mountainous terrain with an explicit cloud model. Part I: Two-dimensional sensitivity experiments. *J. Appl. Meteor.,* **31,** 26–50.

Mossop, S. C., and A. Ono, 1969: Measurements of ice crystal concentrations in clouds. *J. Atmos. Sci.,* **26,** 130–137.

——, ——, and E. R. Wishart, 1970: Ice particles in maritime clouds near Tasmania. *Quart. J. Roy. Meteor. Soc.,* **96,** 487–508.

——, R. E. Cottis, and B. M. Bartlett, 1972: Ice crystal concentrations in cumulus and stratocumulus clouds. *Quart. J. Roy. Meteor. Soc.,* **98,** 105–123.

Parish, T., 1982: Barrier winds along the Sierra Nevada mountains. *J. Appl. Meteor.,* **21,** 925–930.

Rangno, A. L., and P. V. Hobbs, 1991: Ice particle concentrations and precipitation development in small polar maritime cumuliform clouds. *Quart. J. Roy. Meteor. Soc.,* **117,** 207–241.

Rauber, R. M., 1992: Microphysical structure and evolution of a central Sierra Nevada orographic cloud system. *J. Appl. Meteor.,* **31,** 3–24.

Reynolds, D. W., and A. S. Dennis, 1986: A review of the Sierra Cooperative Pilot Project. *Bull. Amer. Meteor. Soc.,* **67,** 513–523.

Rogers, D. C., 1982: Field and laboratory studies of ice nucleation in winter orographic clouds. Ph.D. dissertation, Dept. of Atmospheric Science, Univ. of Wyoming, Laramie, 161 pp.

——, 1988: Development of a continuous flow thermal gradient diffusion chamber for ice nucleation studies. *Atmos. Res.,* **22,** 149–181.

Rosinski, J., and G. Morgan, 1988: Ice-forming nuclei in Transvaal, Republic of South Africa. *J. Aerosol Sci.,* **19,** 531–538.

Saunders, C. P. R., and S. Al-Juboory, 1988: A dynamic processing chamber for ice nuclei filter samples. *12th International Conf. on Atmospheric Aerosols and Nucleation,* Vienna, 697–700.

Schaller, R. C., and N. Fukuta, 1979: Ice nucleation by aerosol particles: Experimental studies using a wedge-shaped ice thermal diffusion chamber. *J. Atmos. Sci.,* **36,** 1788–1802.

Tomlinson, E. M., and N. Fukuta, 1985: A new horizontal gradient, continuous flow, ice thermal diffusion chamber. *J. Atmos. Oceanic Technol.,* **2,** 448–467.

Tripoli, G. J., and W. R. Cotton, 1981: The use of ice–liquid water potential temperature as a thermodynamic variable in deep atmospheric models. *Mon. Wea. Rev.,* **109,** 1094–1102.

——, and ——, 1982: The Colorado State University three-dimensional cloud/mesoscale model—1982. Part I: General theoretical framework and sensitivity experiments. *J. Rech. Atmos.,* **16,** 185–220.

——, and ——, 1989: Numerical study of an observed orogenic mesoscale convective system. Part 1: Simulated genesis and comparison with observations. *Mon. Wea. Rev.,* **117,** 273–304.

Vali, G., 1974: Contact ice nucleation by natural and artificial aerosols. *Conf. Cloud Physics,* Tucson, Amer. Meteor. Soc., 34–37.

——, 1976: Contact-freezing nucleation measured by the DFC instrument. *Third International Workshop on Ice Nucleus Measurements.* Laramie, Univ. of Wyoming, 159–178.

——, 1985a: Atmospheric ice nucleation—A review. *J. Rech. Atmos.,* **19,** 105–115.

——, 1985b: Nucleation terminology. *J. Aerosol Sci.,* **16,** 575–576.

Young, K. C., 1974a: The role of contact nucleation in ice phase initiation in clouds. *J. Atmos. Sci.,* **31,** 768–776.

——, 1974b: A numerical simulation of wintertime, orographic precipitation: Part I. Description of model microphysics and numerical techniques. *J. Atmos. Sci.,* **31,** 1735–1748.

Zamurs, J., G. Lala, and J. Juisto, 1977: Factors affecting ice nucleus concentration measurements with a static vapor-diffusion chamber. *J. Appl. Meteor.,* **16,** 419–424.